Low-Speed Oblique Impact Response of Adhesively Bonded Dissimilar Single-Lap Joints

M. Gokhan Atahan[1] and M. Kemal Apalak[2]

Abstract: Adhesively bonded joints are widely preferred for joining similar and dissimilar materials due to the mechanical advantages they provide. As the demand for the adhesively bonded method increases, it is necessary to determine the behavior of joints under impact loads for joint design. The aim of this study was to investigate the low-speed oblique impact behavior of dissimilar single-lap joints and the effect of plastic deformation ability and strength of the adherends [(Top) Al 2024-T3–(Bottom) Al 5754-0, (Top) Al 5754-0–(Bottom) Al 2024-T3], overlap lengths (25, 40 mm), and impact energy (3, 11 J) on adhesive damage. The behavior of the joints determined by the numerical model under low-speed oblique impact was compared with experimental results. Considering the contact force-time, contact force-displacement, and adhesive damage, the numerical model was reasonably compatible with the experimental results. The damage initiation and propagation in the adhesive layer were determined by three-dimensional explicit finite-element analysis. In order to obtain suitability for the damage mechanism by observing the experimental bonding damage surfaces, the adhesive region was divided into three zones, the upper and lower adhesive interfaces and a middle adhesive layer between them. The different strength and plastic deformation ability of the adherends had a significant effect on the adhesive damage initiation and propagation. In the case of high strength and low deformation ability of the adherend material (Al 2024-T3) contacting with the impactor, a reduction of the adhesive damage occurred due to the deformation of the adherend material (bottom adherend) with low strength and high deformation capability. The oblique impact load and the different mechanical properties of the adherends greatly affected the adhesive damage initiation and propagation of single-lap joints. **DOI: 10.1061/(ASCE)AS.1943-5525.0001472.**

Author keywords: Low speed impact; Oblique impact; Single-lap joint; Cohesive zone model; Adhesive failure; Dissimilar joint.

Introduction

In engineering design, materials with different properties are used together while considering objectives such as lightness and high strength. The adhesively bonded joining method is used effectively in joining materials with different mechanical and chemical properties. This increased interest in bonding joints led to the development of adhesives with high strength and ductility. The development in adhesive technology plays an important role in the joining of materials that cannot be combined with conventional joining methods (Kinloch 2012; Mittal 2012; Adams et al. 1997). Adhesive joints are widely preferred in aerospace industrial applications because they allow different adherends to be combined. The increase in the use of adhesive joints has led many researchers to determine the behavior of adhesively bonded dissimilar joints under quasistatic and dynamic loads. Researchers focus especially on the damage analysis of adhesive joints under quasistatic and dynamic loads. Many research groups have also developed numerical models as well as experimental studies to predict adhesive damage.

Sun et al. (2018) experimentally studied the fracture characteristic of dissimilar adhesive joints under tensile loads. They used the digital image correlation (DIC) method to detect adherend deformation and fracture processes of the adhesive joints. It was reported that when adherends undergo elastic deformation, stiffness of the adherend affects joint stiffness and joint fracture development. Jairaja and Naik (2019) investigated the strength analysis and failure type of dissimilar single-lap joint with single and dual adhesive bond experimentally and numerically. They used two different types of adherends, carbon fiber reinforced polymer (CFRP) and aluminum, and adhesives (Araldite 2015 and AV138). Peeling and shear stresses reached maximum value at the ends of the bonded joint. In addition, the result was obtained that the use of dual adhesive increases bond performance. Chen et al. (2020) studied the effects of overlap length, rivet diameter, and adhesive thickness on failure progression stages of hybrid single-lap joints (CFRP/Al6061-T6) under quasistatic loads using the digital image correlation technique. They reported that the joint type significantly affected the peak load, whereas the lap length and adhesive thickness had a limited effect on the failure modes. Kanani et al. (2021) investigated the effect of joint configuration (scarf joints, stepped-lap joints, half-lap splice joints, and single-lap joints) on the joint strength, damage type, and stress distribution of adhesively dissimilar joints experimentally and numerically. They divided the adhesive region into three layers in the numerical model. The cohesive element COH2D4 in the mesh structure was used between the adherends and adhesive, and the CPE4R element type was used between these two cohesive regions. According to the experimental and numerical damage analysis, they determined that failure always initiates at the polyphthalamide (PPA)-adhesive interface for multimaterial joints (Al 6082-T6-PPA). They also reported that lower adherend stiffness significantly affected the strength of the entire joint.

---

[1] Research Assistant, Dept. of Mechanical Engineering, Abdullah Gul Univ., Kayseri 38080, Turkey (corresponding author). ORCID: https://orcid.org/0000-0002-8180-5876. Email: mithatgokhan.atahan@agu.edu.tr

[2] Professor, Dept. of Mechanical Engineering, Erciyes Univ., Kayseri 38039, Turkey. ORCID: https://orcid.org/0000-0002-3263-5735. Email: apalakmk@erciyes.edu.tr

Note. This manuscript was submitted on January 27, 2022; approved on May 11, 2022; published online on July 7, 2022. Discussion period open until December 7, 2022; separate discussions must be submitted for individual papers. This paper is part of the ***Journal of Aerospace Engineering***, © ASCE, ISSN 0893-1321.

The behavior of adhesive joints under impact loads may be different from the behavior under static loads due to the mechanical properties of the adhesive and adherends affected by the strain-rate and inertia effects. The adhesive, which is polymeric material, has ductile and high strength under static or quasistatic loads, whereas it can have low energy absorption capability by showing brittle features under impact loads. In industries such as automotive and aviation, where security is at a high level, it is important to determine the behavior of adhesive joints under impact loads. When the literature was examined, it was seen that the studies focused on the investigation of the behavior of adhesive joints under normal impact (Machado et al. 2018b; You et al. 2020). However, during an operation, adhesive joints can be exposed to oblique impact loads. An oblique impact load can affect the initiation and propagation of the adhesive damage, and the effect of the oblique impact load on the joint behavior has not yet been fully determined. Studies on oblique impact are generally focused on the behavior of various materials and structures rather than adhesive joints. There are some studies about the behavior of various materials and structures under oblique dynamic load, and the findings were shared in scientific studies. In addition, the dynamic behavior of dissimilar joints has been studied by many researchers (Yildirim and Apalak 2011; Hazimeh et al. 2015; Kadioglu and Adams 2015; Ozdemir and Oztoprak 2017; Boling and Dongyun 2018; Liao et al. 2013; Dhaliwal and Newaz 2021).

Machado et al. (2018a) numerically studied the behavior of mixed adhesive single-lap joints under impact loads for the automotive industry. Their study aimed to improve the mechanical performance of the joint by using adhesives with different mechanical properties in the overlap region. They used the cohesive zone model in their work and reported that the use of the cohesive model was a suitable technique for modeling and predicting the behavior of mixed adhesive joints subjected to quasistatic and impact loading. However, because the plasticity in ductile adhesives could not be reflected in the cohesive zone model, there was a difference between the numerical and experimental results for ductile adhesive. Avendaño et al. (2016) studied the behavior of single-lap joints with dissimilar lightweight adherends and a crash-resistant epoxy adhesive under quasistatic and impact loading for various temperatures. They developed a numerical model to estimate the joint strength under both quasistatic and impact loads. The cohesive zone model was used in the numerical model of the adhesive region. Although there was good agreement between the experimental and numerical results under quasistatic loads, under impact loads, there was moderate agreement between the experimental and numerical results. Inertia effects and changing in material behavior under impact loads affected the agreement between the experimental and numerical results. It was concluded that the joint behavior was significantly affected by the mechanical properties of the adherend material. Valente et al. (2019) numerically studied the behavior of joints under tensile impact loads with three different adhesives using cohesive zone modeling. They reported that there was good agreement between numerical, numerical reference, and experimental curves; however, experimental failure displacement was much higher than in the numerical result. They also stated that the adherend material had a significant effect on single-lap joints under impact load. It was stated that if the adherend material had low stiffness and significantly higher buckling, less uniform stress distribution occurs. Machado et al. (2019) investigated the behavior of dissimilar single-lap joints using composite and aluminum under quasistatic and impact loads. They found that the performance of the dissimilar joints, taken into account for maximum load, was limited by aluminum deformation in all test samples, and aluminum–aluminum similar joints absorbed the most energy for all temperatures in quasistatic test conditions. Li et al. (2020) carried out an experimental and numerical study on the cohesive failure, energy absorption, and postload-carrying capacity of adhesively single-lap joints for four different temperatures and four different impact energies. In their study, the cohesive zone model was used in the adhesive region, and they reported that this model was successful in predicting both the postload-bearing capacity of the adhesive joints and impact damage. They reported that under the transverse impact load, the stress in the adhesive region increased toward the edges because the initiation of damage in the adhesive joints was seen at the edges. Lißner et al. (2020) examined the rate-dependent failure behavior of multimaterial (carbon fiber–reinforced polymers and titanium alloy Ti-6Al-4V) adhesively bonded structures experimentally and numerically for three deformation modes. Considering the experimental observations of the fracture modes studied, they concluded that there was a decrease in fracture energy with increasing loading rate. They also reported that numerical simulations of fracture modes for adhesive joints could accurately predict the experimental behavior. Machado et al. (2020) numerically studied the behavior of adhesive joints with composite and aluminum adherends under quasistatic and impact loads. They also evaluated the effect of the geometric properties of the joint such as the adhesive layer thickness, overlap length, and adherend thickness on joint behavior. They used the cohesive zone model in the composite and adhesive numerical model to determine adhesive and delamination damage. The impact and quasistatic models they developed were reasonably able to predict the mechanical behavior of most of the joints examined. They reported that joint behavior could be predicted using advanced cohesive models that minimize the need for experimental testing.

In the literature, studies on oblique impact are generally focused on energy damping and thin-walled structures. Song (2013) numerically examined windowed square tubes under oblique impact loads. The parametric parameters used in this study were load angle, width, and height of window, and impact speed. Song also proposed a new design method that can effectively increase the critical load angle of the tube without its energy absorption capacity. It was found that the energy absorption of the tube decreases with increasing load angle and decreases significantly when the collapse mode changes from axial to bending collapse. It was also reported that as the window width increases, the critical load angle decreases, and the window height and impact speed do not have a significant influence on the critical load angle. Ivañez et al. (2015) experimentally examined the behavior of composite sandwich plates under low-speed oblique impact. The experimental impact behavior of composite sandwich structures was investigated for 0° (normal impact to the surface), 5°, 10°, and 15° impact angles. They investigated the effects of different impact angles and energies on maximum contact force, maximum contact time, absorbed energy, maximum displacement of the impactor, and the damaged area. There was no significant difference in the results of the investigated parameters for impact angles less than 15°. As the experimental conditions became difficult at impact angles above 50°, they developed a numerical model and analyzed the impact behavior of the sandwich structure. They reported that as the impact angle increased, the damaged area and the maximum contact force decreased. Alkhatib et al. (2018) numerically studied the performance of thin-walled corrugated tapered tubes (CTTs) under oblique impact loading conditions. The effect of loading angles on initial peak force, mean crashing force, energy absorption, and specific energy absorption was investigated in their study. They stated that increasing the impact angles caused a decrease in impact performance, and when the impact angle increased from 0° to 40°, an approximate 54% reduction in energy absorption and specific energy absorption was observed. Pascal et al. (2018) numerically studied the effect of low-velocity normal and oblique impacts on sandwich panels having woven composite skins and a polyurethane foam core. The numerical results were good enough to represent the type of damage experimentally observed. Moreover, they reported that the analysis of the results helped to understand better the mechanisms that led to the final fracture shape.

When the literature was examined, the behavior of materials and structures under oblique impact is different from that under normal impact loads. The shear stress, which increases with the impact angle, is effective on both the damage areas and the initiation and propagation of the damage. Although the behavior of many materials and engineering structures under oblique impact has been determined, studies on the behavior of adhesive joints under oblique impact load are limited. The adhesive bonding method is particularly suitable for combining dissimilar materials. In this study, the behavior of dissimilar aluminum single-lap joints with adherends with different mechanical properties under low-speed oblique impact loads was investigated, and the initiation and propagation of adhesive damage were examined comparatively.

Experiment

Specimen Preparation

Al 2024-T3 and Al 5754-0 were used as adherends, and Araldite 2015 was used as an adhesive in single-lap joints. The adherend materials were selected to have different mechanical properties. The adhesive (Araldite 2015) used in the study has a high impact resistance and medium ductility. The main purpose in this selection was to determine the effect of dissimilar adherend materials with different mechanical properties under oblique impact loads on the initiation and propagation of adhesive damage. Rectangular pieces were cut from a 2-mm-thick sheet with a guillotine. Before the bonding process, the bonding surfaces were cleaned with ethanol. Araldite 2015 adhesive was applied on the cleaned surfaces and evenly spread over the surface [Fig. 1(a)].

It was then placed between the bonding apparatus [Fig. 1(b)]. The bonding apparatus consisted of an upper and lower part with four 4.2-mm-thick washers between the layers, which adjusted the adhesive thickness. The single-lap joints between the apparatus were kept at room temperature until cured [Fig. 1(c)]. The impact test apparatus was manufactured for each of the three impact angles (θ: 10°, 20°, 30°). Each impact apparatus ensured that the impactor applied an impact load in the middle of the joint, and the effective length (L) of the joint was 160 mm (Fig. 2).

Method

In order to determine the effect of impact angle (θ: 10°, 20°, 30°), overlap length (b: 25, 40 mm), plastic deformation ability of adherend [(Top) Al 2024-T3–(Bottom) Al 5754-0, (Top) Al 5754-0–(Bottom) Al 2024-T3], and impact energy (E: 3, 11 J), low-speed impact tests were applied to adhesively bonded single-lap joints using a Fractovis Plus impact test machine (Erciyes Univ. Manufacturing Laboratory, Kayseri, Turkey). The apparatus for each impact angle was manufactured to apply impact to the single-lap joint at the desired angle. The effective (L) and holding length of the joints were 160 and 20 mm, respectively [Fig. 2(a)]. In addition, to determine the effect of overlap length values on impact behavior, overlap lengths (b) of 25 and 40 mm were determined for impact tests (Fig. 2). The width of the single-lap joints was 25 mm for all specimens. Impact energies of 3 and 11 J were applied to the single-lap joints with a semicylindrical impactor with a radius of 5 mm, a width of 25 mm, and a total mass of 5.302 kg. The contact force–time and force–displacement graphs of the joints were obtained from the impact test machine. As a result of the impact tests, complete, partial, and no separation conditions of the joints were observed. The partially damaged joint specimens were forced to completely separate from the marked adhesive damage by hand. Then, the adhesive damage caused by impact load in all the joints was examined, with photographs of the fracture surfaces. The main aim of this study was to investigate the behavior of dissimilar single-lap joints under oblique impact loading and to compare adhesive damage initiation and propagation. It also aimed to investigate the effect of the position of the adherends with different strength and plastic ductility [(Top) Al 2024–(Bottom) Al 5754, (Top) Al 5754–(Bottom) Al 2024] on adhesive damage.

Finite-Element Model

Performing impact tests, taking measurements, and examining damage patterns may require expensive testing and imaging equipment. At this point, the finite-element method is a suitable solution due to the advantages it provides. The finite-element method provides not only material, time, and cost savings but also enables the analysis of experimentally difficult mechanical tests. ABAQUS/Explicit three-dimensional finite-element analysis was used to examine the behavior of adhesive joints under low-speed oblique impact and to determine the initiation and propagation of adhesive damage. Numerical results were verified by experimental results, and time-dependent adhesive damage was determined, which is difficult to visualize experimentally. The impact analysis of the adhesively bonded single-lap joints was implemented by considering two dissimilar joint configurations of (Top) Al 2024–(Bottom) Al 5754 and (Top) Al 5754–(Bottom) Al 2024; three different impact angles (θ) of 10°, 20°, and 30°; two different overlap lengths (b) of 25 and 40 mm; and two different impact speeds of (v) 1.064 and 2.037 m/s. No geometric and mass scales were used in the numerical analysis. The dimensions of the single-lap joint and impactor mass were defined in accordance with the experimental study. The numerical model of the adhesive region was the most

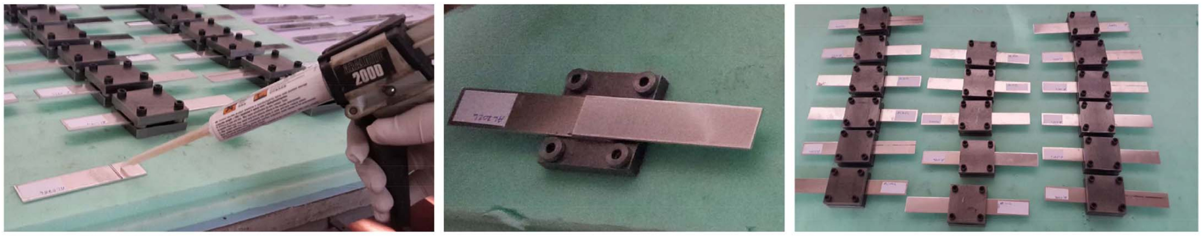
(a) (b) (c)

Fig. 1. Specimen preparation stages: (a) applying adhesive; (b) placement of joint in apparatus; and (c) keeping the joints in the apparatus.

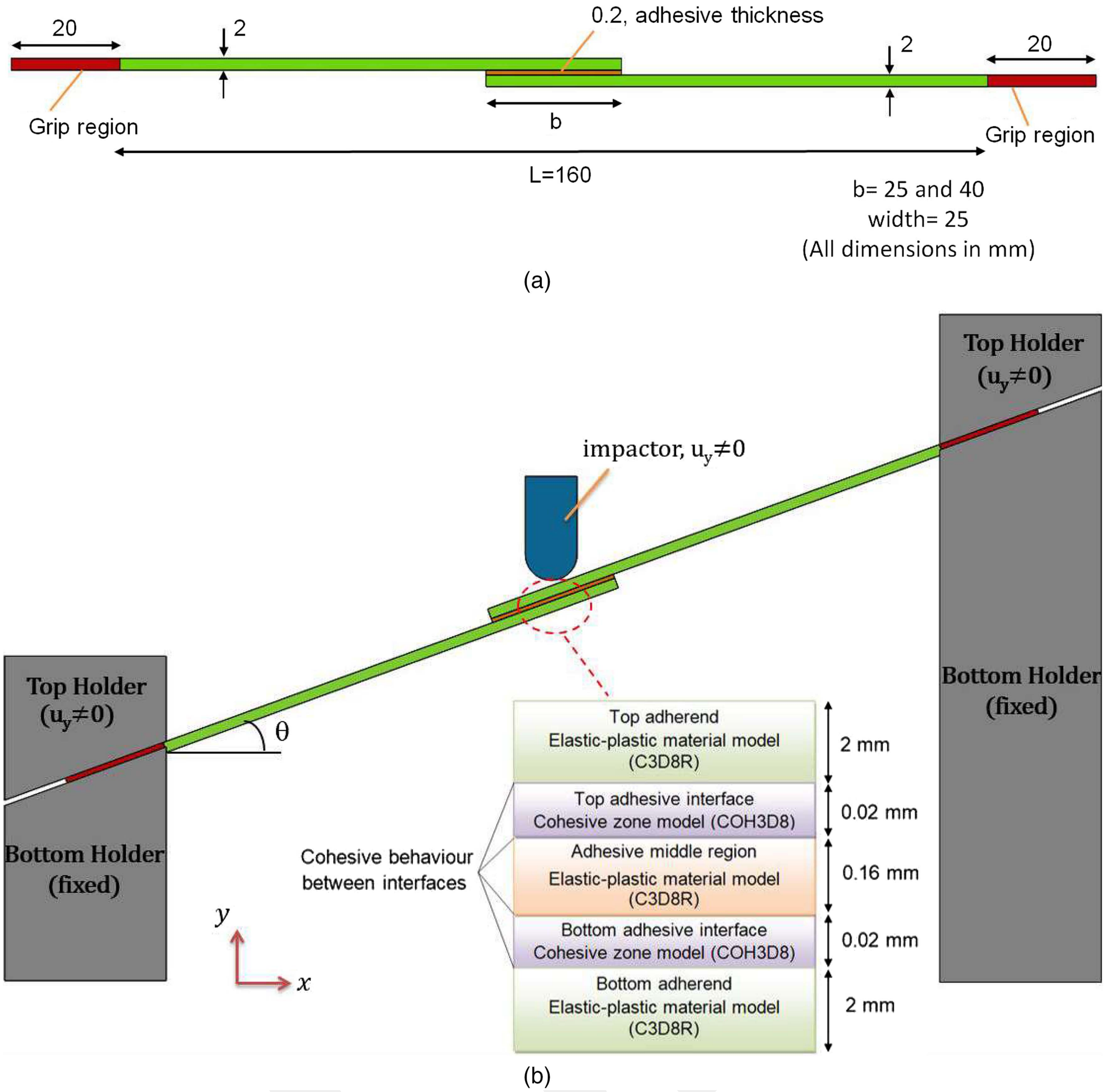

Fig. 2. (a) The geometry and dimensions of dissimilar single-lap joint; and (b) boundary conditions and numerical modeling structure of adhesive and adherends.

critical part in the analysis. Araldite 2015 adhesive is a medium-ductility adhesive and has a high plastic deformation capacity [Fig. 3(c)].

In addition, it was observed that the damage progressed within the adhesive layers, thanks to the fracture surfaces of the adherends. Considering these two factors, the adhesive region was modeled by dividing it into three parts [Fig. 2(b)], whereas the interfaces of the adhesive, which were in contact with the upper and lower adherends, were modeled with the cohesive zone model, and the middle region between these two cohesive regions was modeled with the elastic–plastic material model. Plastic behavior in the adhesive region was described by the isotropic hardening plasticity model [ABAQUS (2018)]. In this material model, the stress–strain data obtained from the tensile test of the adhesive were used. Elastic–plastic behavior in the adhesive region has been applied by many researchers with a similar material model approach (Yildirim and Apalak 2011; Bayramoglu et al. 2021; Nejad et al. 2022; Ri et al. 2022).

The cohesive zone model was based on the elastic traction-separation behavior of the material. Therefore, the use of the elastic–plastic material model in the middle region of the adhesive enabled the plastic behavior of the adhesive to be reflected in the analysis. In the cohesive zone model used in adhesive interfaces, the initiation of damage was evaluated according to the maximum nominal stress criteria. The damage began when any of the traction rates in the normal and two shear directions reached one value, as follows [ABAQUS (2018)]:

$$\max\left\{\frac{\langle t_n\rangle}{t_n^o}, \frac{t_s}{t_s^o}, \frac{t_t}{t_t^o}\right\} = 1 \tag{1}$$

$$t_n = (1-D)\bar{t}_n, \quad if\ \bar{t}_n \geq 0 \tag{2}$$

$$t_n = \bar{t}_n, \quad if\ \bar{t}_n < 0 \quad (\text{no damage}) \tag{3}$$

$$t_s = (1-D)\bar{t}_s \tag{4}$$

$$t_t = (1-D)\bar{t}_t \tag{5}$$

where $\bar{t}_n$, $\bar{t}_s$, and $\bar{t}_t$ = predicted stress components in normal and two shear directions, respectively, without any damage;

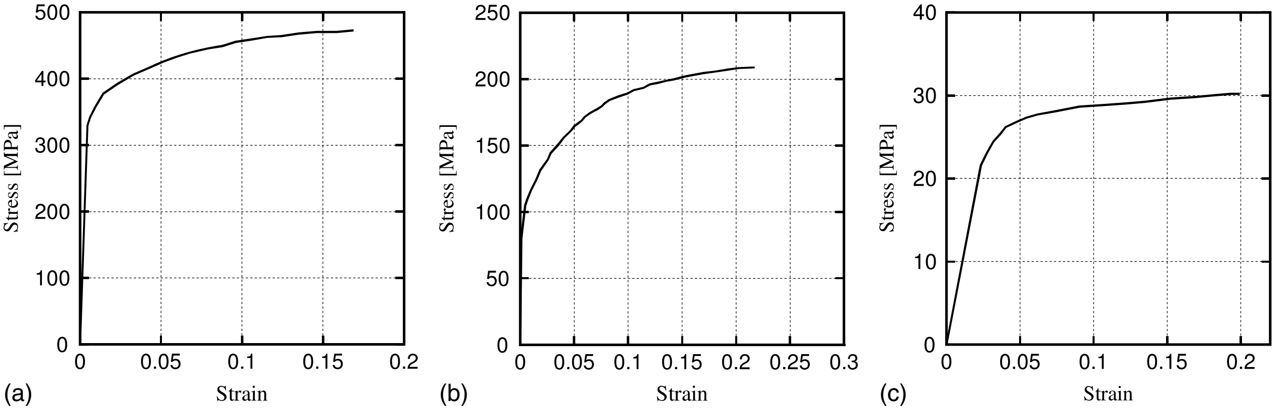

Fig. 3. Stress–strain curves of (a) aluminum 2024-T3; (b) aluminum 5754-0; and (c) epoxy adhesive (Araldite 2015). (Data from Yildirim and Apalak 2011, Atahan and Apalak 2017, Araldite 2015.)

and D = damage parameter, and it is expressed in terms of the effective interface separation (δ_m) expression as follows:

$$\delta_m = \sqrt{\langle\delta_n\rangle^2 + \delta_s^2 + \delta_t^2} \tag{6}$$

for a linear damage evolution

$$D = \frac{\delta_m^f(\delta_m^{\max} - \delta_m^o)}{\delta_m^{\max}(\delta_m^f - \delta_m^o)} \tag{7}$$

for an exponential damage evolution

$$D = 1 - \left\{\frac{\delta_m^o}{\delta_m^{\max}}\right\}\left\{1 - \frac{1 - \exp\left(-\alpha\left(\frac{\delta_m^{\max} - \delta_m^o}{\delta_m^f - \delta_m^o}\right)\right)}{1 - \exp(-\alpha)}\right\} \tag{8}$$

where δ_n, δ_s, and δ_t = interfacial separations for normal and two shear directions, respectively; δ_m^o, δ_m^f, and $\delta_m^{\max}$ = effective interfacial separation at failure initiation, effective interfacial separation at failure, and maximum effective interfacial separation, respectively (ABAQUS 2018; Camanho and Dávila 2002); and α = nondimensional damage parameter that represents the rate of damage evolution. Whereas the value of 0 represents linear variation, an increase in this value causes the exponential effect to become more apparent in the damage evolution. Because the nondimensional damage parameter α affects the damage evolution rate, the contact force–time variations and the amount of adhesive damage are affected by the change of this value. Therefore, considering the contact force–time variation and the axial separation length, the damage evolution parameter α was tested for each impact angle between zero and eight values. The damage evolution parameter α was determined as 4 by considering the agreement between the experimental and numerical results, and this value was kept constant in all impact analyses. The cohesive behavior defined in the upper and lower regions of the adhesive was used to predict interfacial damage. Table 1 presents the cohesive material properties of the Araldite 2015, which were determined by Campilho et al. (2013).

The damage evolution of adhesive determined with a failure displacement value of 0.065 mm measured the mixed mode flexure (MMF) test by Wong (2013). The MMF test geometry is similar to single-lap joints under bending impact load and includes failure modes I and II. For the elastic–plastic modeled part in the middle of the adhesive, a failure strain of 0.17 and failure displacement of 0.065 mm were used for damage initiation and evolution, respectively. The failure strain value of adhesive was obtained from the stress–strain curve of the adhesive [Fig. 3(c)]. Cohesive and mechanical properties of adhesive were determined by various mechanical tests such as tensile, shear, double cantilever beam (DCB), end notched flexure (ENF), and MMF tests. It was determined that these mechanical tests were applied at room temperature, and the specimens were prepared according to the manufacturer's recommendations (Yildirim and Apalak 2011; Campilho et al. 2013; Wong 2013). Similarly, the adhesive joints were prepared according to the manufacturer's recommendations, and the impact tests were carried out at room temperature in this study. In the cohesive zone model, it is important to determine the mesh element size, interface stiffness, and damage parameters appropriately. Zhao et al. (2014) examined the effects of interface stiffness, cohesive element size, viscosity coefficient, and interface strength on cohesive behavior. It can be assumed that the initial stiffness is equal to the elastic and shear modulus for the thin adhesive layer ($K_{nn} = E$, $K_{ss} = G$, $K_{tt} = G$) (Campilho et al. 2013, 2008, 2010). Normal and shear tractions were evaluated as equal to the tensile and shear strength of the adhesive, respectively (Campilho et al. 2013; Machado et al. 2019; Araújo et al. 2017). Damage initiation is determined by traction values (normal and shear), whereas damage propagation can be estimated by fracture energy or failure displacement value. In this study, damage propagation was determined by the failure displacement value obtained from the MMF test. Considering the cohesive region, mesh sensitivity was tested with an Al 5754 (Top)–Al 2024 (Bottom) single-lap joint with 10° impact angle, 40 mm overlap length, and 3 J impact energy. Axial separation length values were determined as 26, 24.5, and 23.6 mm for the mesh sizes of 1, 0.5, and 0.2 mm, respectively ($\Delta_E = 20$ mm).

Table 1. Cohesive and mechanical properties of Araldite 2015 adhesive used for CZM

E (GPa)	G (GPa)	υ	t_n^o (MPa)	t_s^o (MPa)	t_t^o (MPa)	δ_f(MMF) (mm)	ρ (kg/m^3)
1.85	0.56	0.33	21.63	17.9	17.9	0.065	1,400

Source: Data from Campilho et al. (2013); Wong (2013).

Table 2. Mechanical properties of adherends (Al 2024-T3 and Al 5754-0)

Materials	Density $(\mathrm{kg/m^3})$	Modulus of elasticity (GPa)
Al 2024-T3	2,780	73
Al 5754-0	2,660	68

Source: Data from Atahan and Apalak (2017).

As the mesh size decreased, the numerical damage estimation converged to the experimental results. However, the numerical analysis time increased as the mesh size decreased. For this reason, all finite-element analyses were carried out considering the 0.2-mm mesh size of the cohesive region. The viscosity coefficient provides the improvement of the convergence of the numerical analyses in the softening stage (ABAQUS 2018; Zhao et al. 2014). No viscous

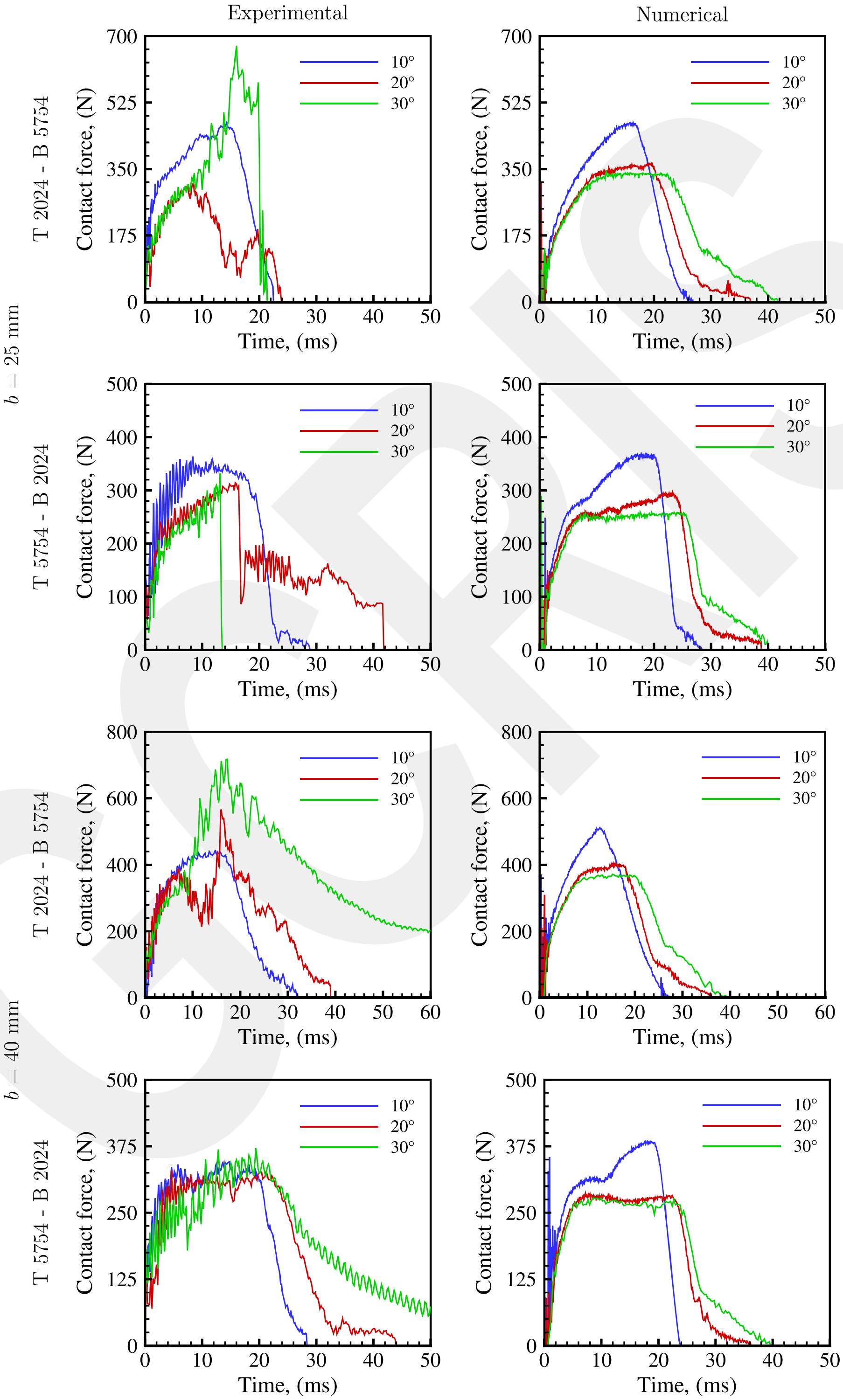

Fig. 4. Experimental and predicted contact force–time diagrams of T Al 2024–B Al 5754 and T Al 5754–B Al 2024 single-lap joints depending on different oblique impact loadings ($b = 25$, 40 mm, $E = 3$ J).

regularization was performed in the numerical analysis because the numerical results were in good agreement with the experimental results. Impact tests of adhesive joints are divided into three groups as low-speed, medium-speed, and high-speed impact (Adams 2021; Machado et al. 2018b). The low-speed impact test is defined with a speed up to 5 m/s (Adams 2021). In impact tests, the strain rate effect becomes more evident with the increase in impact test speed. Because the impact test velocities ($v = 1.064$ and $2.037\ \mathrm{m/s}$) used in this study were low, the influence of strain rate was negligible. Abrate (1998) and Goldoni and Mantovani (2021) stated that the strain rate effect can be neglected for low-speed impact analysis. Therefore, in this study, the material properties obtained from quasistatic mechanical tests were used in the numerical analysis, and the strain rate effect was not taken into account.

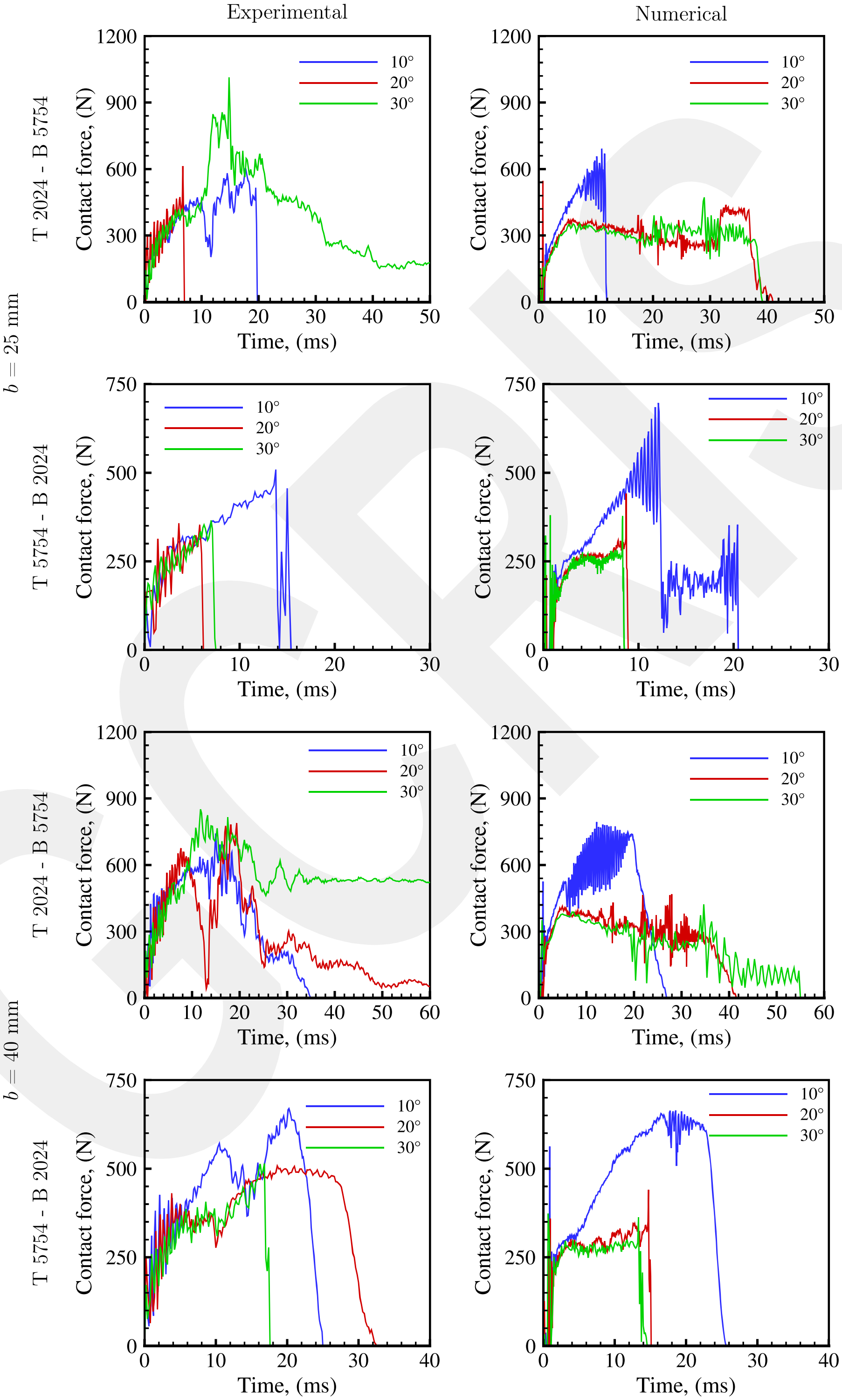

Fig. 5. Experimental and predicted contact force–time diagrams of T Al 2024–B Al 5754 and T Al 5754–B Al 2024 single-lap joints depending on different oblique impact loadings ($b = 25$, 40 mm, $E = 11$ J).

Adhesive interfaces with a thickness of 0.02 mm were modeled with a cohesive element COH3D8, whereas the adhesive middle region of 0.16-mm thickness was modeled with a three-dimensional (3D)–continuum finite-element C3D8R. The mesh structure was set to concentrate from the edges of the joint toward the overlap region using the Bias command. The cohesive surfaces were defined to prevent any numerical error between the continuum and cohesive elements in contact with each other in the adhesive region [Fig. 2(b)]. The impactor, with a total mass of 5.302 kg and a radius of 5 mm, was modeled as Discrete Rigid; a reference point was placed at the center point; and mass and velocity values were defined at this reference point. The impactor was modeled using the R3D4 element type and could only move in the *y*-direction. Aluminum adherend materials were modeled with an elastic–plastic material model using the stress–strain curve [Figs. 3(a and b), Table 2] and used the C3D8R element type in the mesh structure [Fig. 2(b)].

In the finite-element model, a general contact algorithm between the probable contact surfaces of the impactor, adherends, and adhesive was defined. The holder surfaces were roughened to provide better holding. Therefore, whereas a friction coefficient of 0.5 was defined between the specimen and the holders in the analysis, a friction coefficient of 0.25 was defined between the impactor and the specimen. Whereas the movement of the lower holding apparatus was fixed in three axes, only movement of the upper holding apparatus in the *y*-direction was allowed [Fig. 2(a)]. In the experimental test, although the pressure provided by the compressor was constant, the holding pressure applied to the specimen from the top holder decreased as the impact angle increased. In order to determine the holding pressure in the numerical analyses, the holding force components were first calculated with the statics equilibrium equations. Then, the holding pressure values were determined for each impact angle with the preliminary analysis. As a result, 8-bar, 4-bar, and 4-bar pressures were applied between the top holder surface and specimen surface for 10°, 20°, and 30° impact angles, respectively, considering the agreement between the experimental and numerical results.

Results and Discussion

Effective Parameters on Impact Response

The oblique impact behavior of dissimilar single-lap joints was investigated experimentally and numerically. Whereas Al 2024-T3 had high strength and partially low plastic deformation ability, Al 5754-0 had low strength and high plastic deformation capability, and the effect of the configuration of these two materials (top and bottom) on the impact behavior and damage initiation and propagation was studied under oblique impact. In addition, the effects of impact energy and overlap length also were considered. Experimental and numerical contact force–time graphs of T(op) Al 2024–B(ottom) Al 5754 and T(op) Al 5754–B(ottom) Al 2024 single-lap joints with 3 and 11 J impact energies are shown in Figs. 4 and 5.

In T Al 2024–B Al 5754 joints under 3 J impact energy, the contact force decreased with the increase of the impact angle, except for the 30° impact angle. In the numerical results, the contact force value decreased with the increase of the impact angle, whereas the total contact time increased. Because it had a high impact angle of 30°, the impactor slipped on the joint without any adhesive damage to the joint. As the plastic deformation capacity of the underlying material (Al 5754) was high in the T Al 2024-B Al 5754 joint, the joint deformed laterally, and the impactor contacted with the underlying material (Al 5754). As a result, the contact force reached a higher value at an impact angle of 30° in the experimental study. In the T Al 5754-B Al 2024 joint, adhesive damage occurred as a result of the deformation of Al 5754.

Table 3. The experimental and numerical peak contact force ($P_{\max}$), axial separation length (Δ), permanent central deflection (δ) values, and failure type for T Al 2024-B Al 5754 and T Al 5754-B Al 2024 dissimilar single-lap joints

				$P_{\max}$ (N)		Δ (mm)		δ (mm)		
E (J)	*b* (mm)	Joint	θ°	Experimental	Numerical	Experimental	Numerical	Experimental	Numerical	Failure type
3	25	T 2024–B 5754	10	472.4	472.2	0	2.0	10.0	7.9	No
			20	311.9	364.3	0	0	10.0	7.2	No
			30	673.8	342.8	0	0	6.0	6.6	No
		T 5754–B 2024	10	363.7	370.8	15.0	16.6	14.0	11.2	Mixed
			20	314.1	295.9	25.0	18.7	8.0	11.0	Mixed
			30	331.9	289.8	25.0	19.2	8.0	9.2	Top interface
	40	T 2024–B 5754	10	442.4	511.8	15.0	12.3	6.0	6.6	Mixed
			20	566.4	403.6	0	0	6.0	5.2	No
			30	717.9	371.8	0	0	5.0	5.5	No
		T 5754–B 2024	10	345.7	384.7	20.0	23.6	14.0	11.0	Top interface
			20	329.4	286.8	22.0	24.3	13.0	9.8	Top interface
			30	371.7	277.8	26.0	24.6	12.0	8.4	Mixed
11	25	T 2024–B 5754	10	601.2	691.5	25.0	25.0	17.0	17.8	Mixed
			20	613.1	546.9	25.0	0	14.0	26.1	Top interface
			30	1,013.9	471.8	0	0	20.0	23.0	No
		T 5754–B 2024	10	520.01	696.8	25.0	25.0	29.0	29.2	Top interface
			20	357.9	441.3	25.0	25.0	25.0	14.7	Top interface
			30	365.7	380.0	25.0	25.0	20.0	11.7	Top interface
	40	T 2024–B 5754	10	742.5	794.2	0	30.5	18.0	19.3	No
			20	789.4	468.6	0	0	17.0	24.3	No
			30	851.7	422.8	0	0	16.0	22.1	No
		T 5754–B 2024	10	669.3	664.6	27.0	27.6	28.0	26.5	Top interface
			20	507.6	440.7	30.0	40.0	30.0	21.6	Top interface
			30	514.4	373.2	40.0	40.0	21.0	17.5	Top interface

In addition, the lateral contact between the impactor and joint at an impact angle of 30° continued throughout the impact loading, and the contact force could not reach zero because the contact between the impactor and joint was not cut. A higher strength of the material (T Al 2024–B Al 5754) in contact with the impactor led to a higher contact force value. Similarly, the increase in impact energy increased the maximum contact force value. The position of the adherend materials in the joint (top and bottom) significantly affected the impact behavior of the joint. If the material (Al 5754) with high plastic deformation capacity came into contact with the impactor, adhesive damage occurred due to the peeling effect. However, if the plastic deformation capacity of the material (Al 2024) in contact with the impactor was low, little or no adhesive damage occurred in the single-lap joint. With the

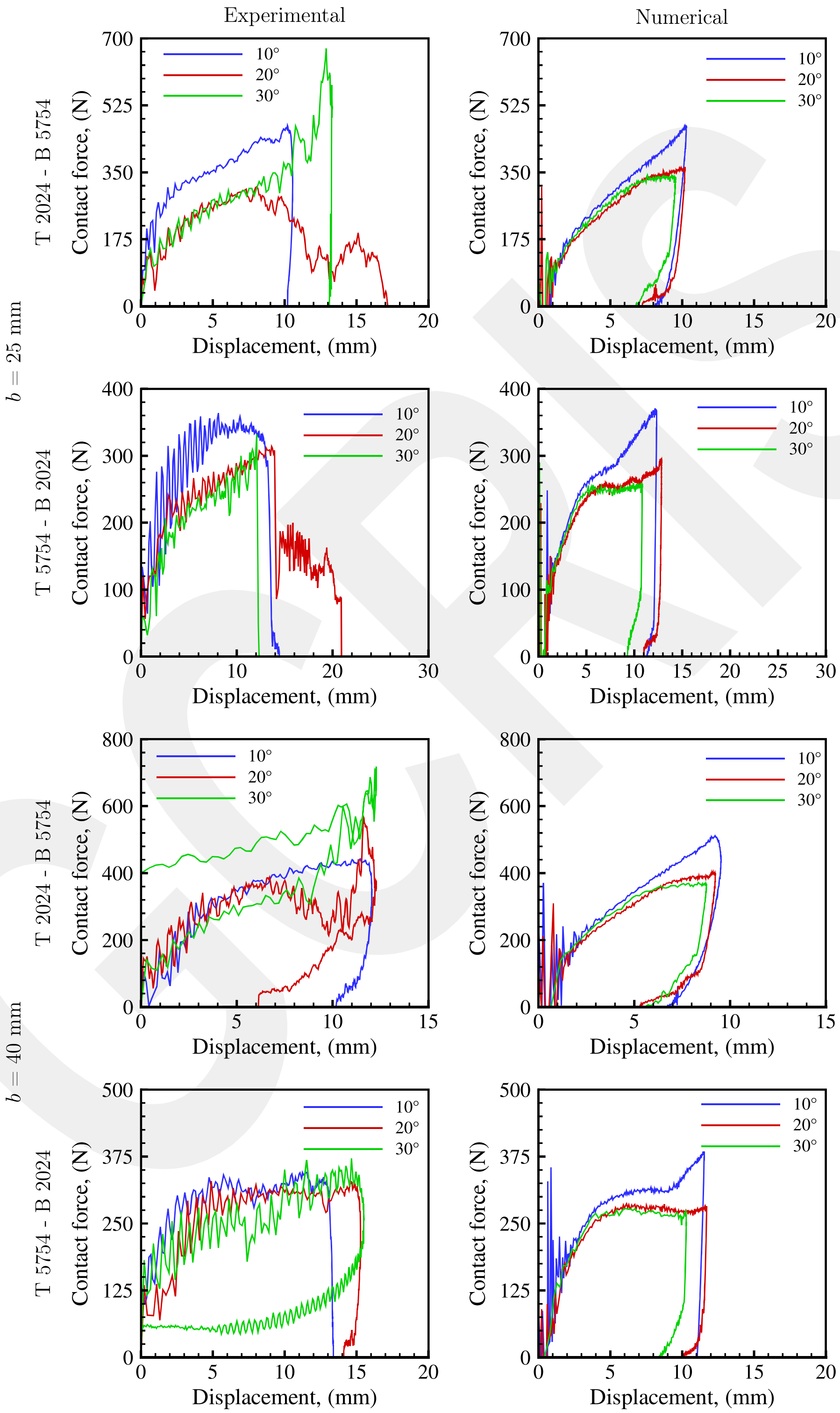

Fig. 6. Experimental and predicted contact force-central deflection diagrams of T Al 2024–B Al 5754 and T Al 5754–B Al 2024 single-lap joints depending on different oblique impact loadings ($b = 25$, 40 mm, $E = 3$ J).

increase in impact angle, the vertical force component applied to the joint decreased, whereas the tangential force component increased. Whereas the vertical force component caused adhesive damage by the peeling effect, the tangential force component damaged the adhesive with a shear effect.

Experimental and numerical maximum contact force ($P_{\max}$), axial separation length (Δ), and vertical deflection (δ) values of the single-lap joints are summarized in Table 3. There was good agreement between the experimental and numerical peak contact force and deflection values. The increase in overlap length did not have a significant effect on the maximum contact force value. In T Al 5754-B Al 2024 joints, the maximum contact force value decreased by 8.7% (experimental) and 21.8% (numerical) with the increase of the impact angle at 25 mm overlap length. The sensitivity of the

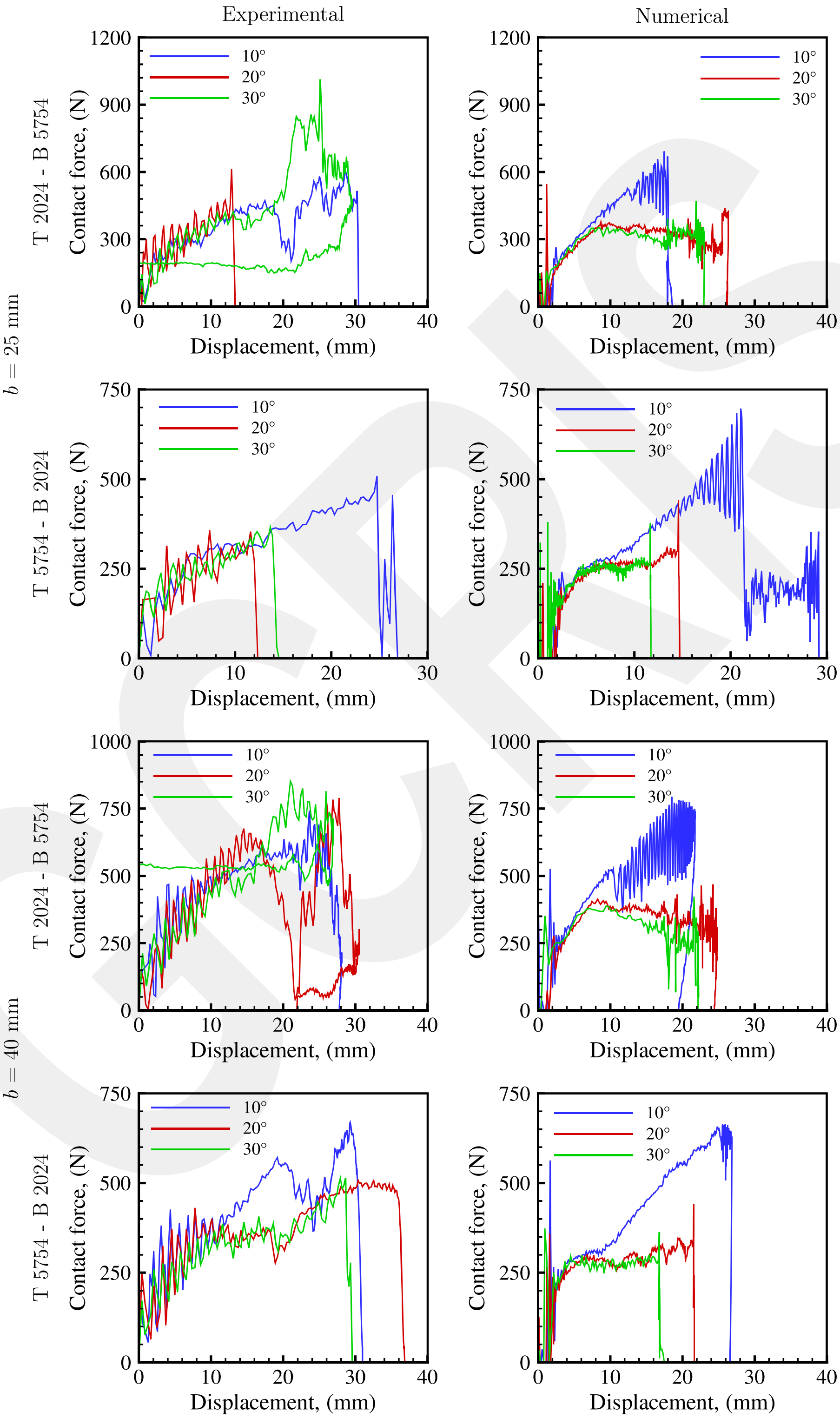

Fig. 7. Experimental and predicted contact force-central deflection diagrams of T Al 2024–B Al 5754 and T Al 5754–B Al 2024 single-lap joints depending on different oblique impact loadings ($b = 25$, 40 mm, $E = 11$ J).

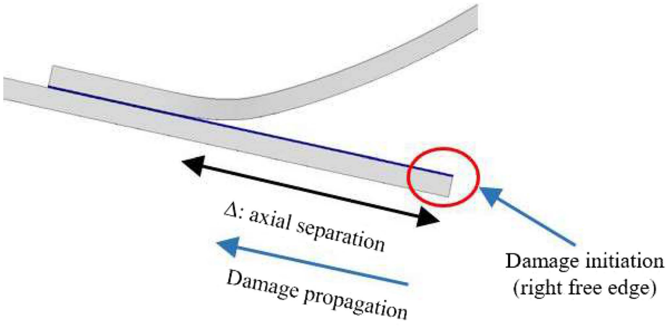

Fig. 8. Demonstration of the adhesive damage initiation and propagation in the lateral region of the overlap.

contact force value to the increasing impact angle became more apparent with the increase of impact energy. The contact force-central deflection graphs of the T A1 2024–B Al 5754 and T A1 5754–B A1 2024 joints are shown in Figs. 6 and 7. The T Al 5754–B Al 2024 joint had more vertical displacement value than the T Al 2024-B Al 5754 joint. Whereas Al 2024 experienced the applied impact energy mostly with elastic deformation, Al 5754 provided the absorption of impact energy by undergoing plastic deformation. Therefore, the presence of the material with high plastic deformation ability (A1 5754) in the part in contact with the impactor in the joint caused the joint to undergo more vertical displacement. In addition, the increase in impact energy caused the joint to experience more vertical displacement. The overlap length of 25 mm was insufficient to meet the 11 J impact energy.

After the contact force reaches the highest level, the impactor rebound phase begins, and from that moment on, the displacement value decreases. Due to the fact that Al 2024 mostly underwent elastic deformation in the T Al 2024–B Al 5754 joints, the decrease in the displacement value in the rebound phase was more than the T Al 5754–B Al 2024 joints. Because the joints were completely separated for 11 J impact energy, no decrease in the displacement value was observed. In the T Al 5754–B Al 2024 joint, more of the impact energy was spent on plastic deformation compared to the T Al 2024–B Al 5754 joint. If the Al 5754, which has a higher plastic deformation capacity, was located at the top of the joint, the amount of impact energy spent on the plastic deformation increased. The adhesive damage in the joints increased with the increase in the impact angle for the T Al 5754–B Al 2024 joints. The T Al 5754–B Al 2024 joints were more sensitive to increased shear stress in the overlap region. The load-carrying capacity of the T Al 5754–B Al 2024 joints decreased as the impact angle increased. Therefore, oblique impact behavior should

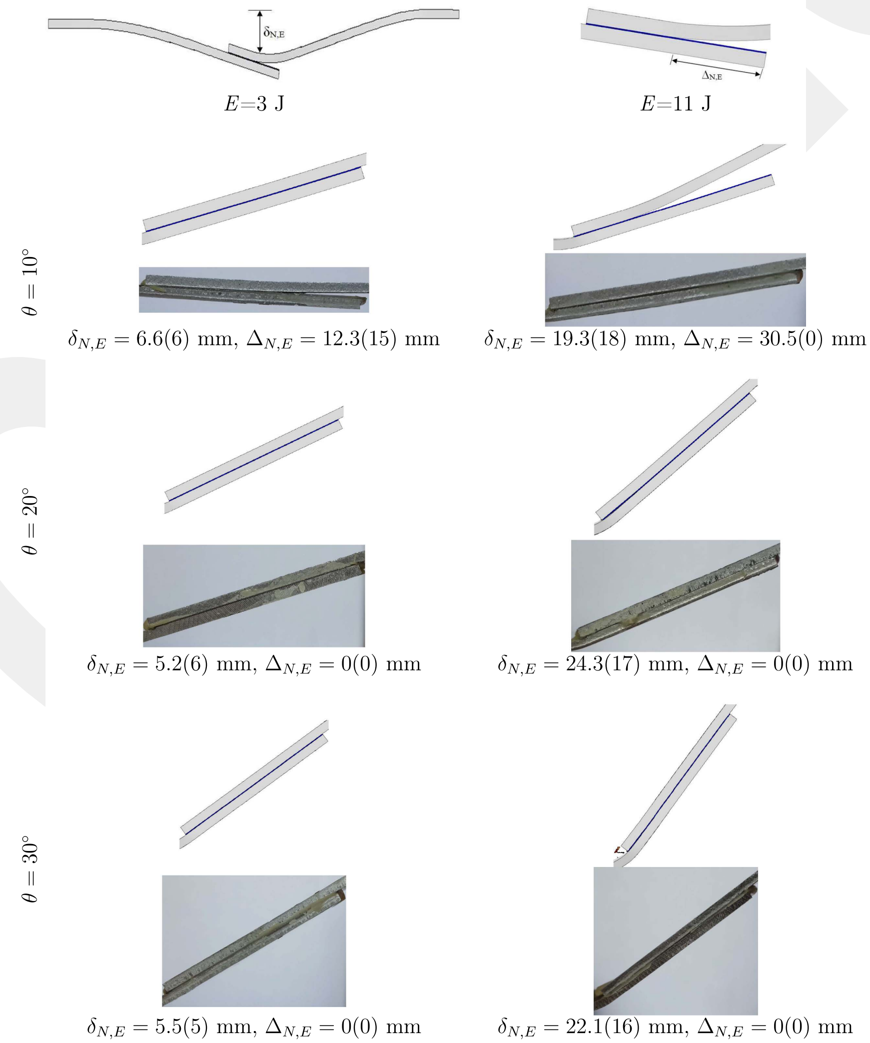

Fig. 9. Experimental (E) and numerical (N) images of the deformed geometries of the T Al 2024–B Al 5754 single-lap joints ($b = 40$ mm).

be taken into account in the design of dissimilar adhesive joints under impact load.

Aluminum adherends undergo deformation, and damage may occur in the adhesive region in the single-lap joints under impact load. Adhesive damage can be characterized as cohesive, interfacial, or mixed. Adhesive damage initiation and propagation of single-lap joints under impact load are schematically shown in Fig. 8.

The experimental and numerical deformed geometries of T Al 2024–B Al 5754 single-lap joints for 40 mm overlap length are presented in Fig. 9. The value $\delta_{N,E}$ indicates the measured numerical and experimental deflections, and $\Delta_{N,E}$ indicates the numerical and experimental axial separation length measured from the lateral region of the overlap (Fig. 8). In addition, the experimental and numerical axial separation lengths and deflections of all joints are included in Table 3. Although the impact angle increased in the T Al 2024–B Al 5754 joints for 3 J impact energy and an overlap length of 25 mm, no adhesive damage occurred. The adhesive damage occurred at only the 10° impact angle for the 40 mm overlap length. There is a material with high strength (Al 2024) in the region that is in contact with the impactor in the joints and a material with a lower strength but high deformation capacity (Al 5754) on the other side of the joint. It ensured that it met applied impact energy with adherend plastic deformation.

In the case where Al 5754 was present in the joint that came into contact with the impactor, a significant amount of adhesive damage occurred due to plastic deformation of the top adherend material (Fig. 10). As Al 5754 was deformed plastically, peeling stress increased in the adhesive region. The position of Al 5754 in the joint directly affected the adhesive damage. Whereas Al 5754 was located at the top of the joint, it caused adhesive damage by deforming with the effect of peeling, and when it was located at the bottom, it underwent plastic deformation and ensured that the impact energy was met without adhesive damage. The tangential component of the contact force was more effective on the adhesive damage with the increase in the impact angle. In the T Al 2024-B Al 5754 joints, despite the increase in the impact angle, adhesive damage did not occur for many impact angles. Whereas the impact energy of 3 J remained low for the Al 2024 adherend to undergo plastic deformation, plastic deformation was evident at 11 J impact energy. However, despite the increase in impact energy (11 J), adhesive damage did not occur in T Al 2024–B Al 5754 joints with an overlap length of 40 mm for oblique impact angles. The overlap length of 25 mm was insufficient for both the T Al 2024–B Al 5754 and T Al 5754–B Al 2024 joints to resist the 11 J impact energy.

Adhesive damage initiated from the right free edge of the top adherend–adhesive interface and propagated toward the left free edge of the overlap. When the axial adhesive separation lengths ($\Delta_{N,E}$) in the joints were examined, the shear stress occurred in the joints increased with the increase of the impact angle, and as a result, the adhesive damage increased. However, a different situation was experienced in the T Al 2024–B Al 5754 joints. Thanks to the high plastic deformation capacity of the Al 5754, the impact energy was absorbed, and thus the shear stress occurred in the overlap region was reduced. As a result, with the increase in the impact angle, adhesive damage increased in the T Al 5754–B Al 2024 joints, whereas adhesive damage did not occur in most of the T Al 2024–B Al 5754 joints. When the deflection values of the joints after the impact test were examined, there was less deflection in

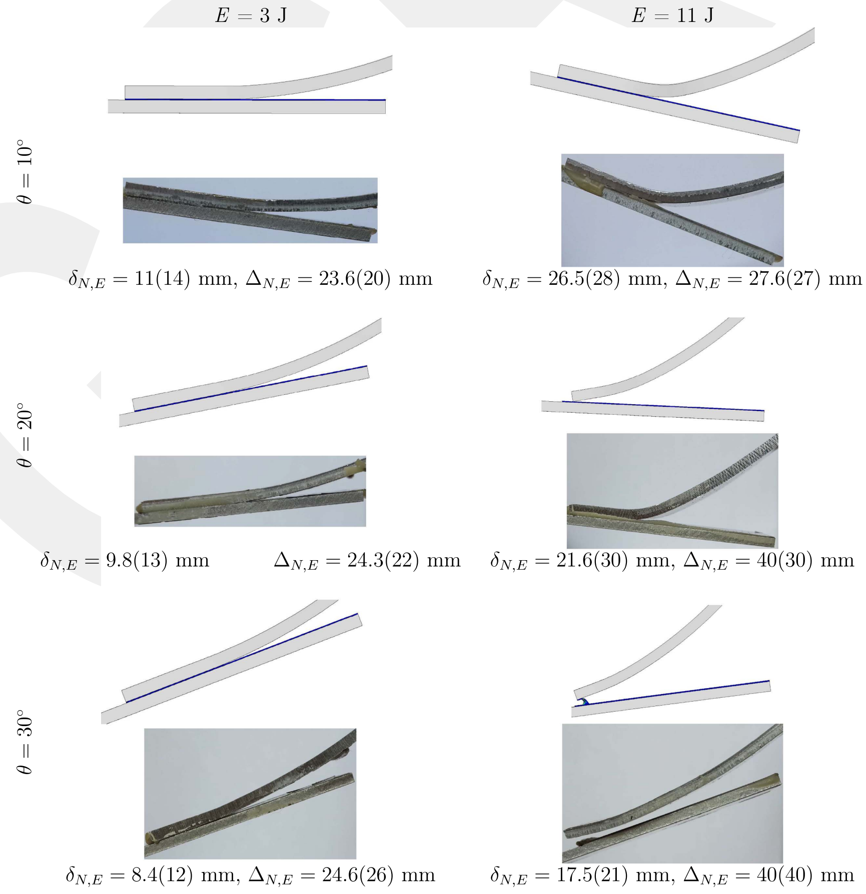

$\delta_{N,E} = 11(14)$ mm, $\Delta_{N,E} = 23.6(20)$ mm

$\delta_{N,E} = 26.5(28)$ mm, $\Delta_{N,E} = 27.6(27)$ mm

$\delta_{N,E} = 9.8(13)$ mm $\Delta_{N,E} = 24.3(22)$ mm

$\delta_{N,E} = 21.6(30)$ mm, $\Delta_{N,E} = 40(30)$ mm

$\delta_{N,E} = 8.4(12)$ mm, $\Delta_{N,E} = 24.6(26)$ mm

$\delta_{N,E} = 17.5(21)$ mm, $\Delta_{N,E} = 40(40)$ mm

Fig. 10. Experimental (E) and numerical (N) images of the deformed geometries of the T Al 5754–B Al 2024 single-lap joints ($b = 40$ mm).

T Al 2024–B Al 5754 joints (Table 3). The presence of a material with low plastic deformation capacity (A1 2024) in the part contacting the impactor decreased the deflection value of the joint. However, the presence of a material with high plastic deformation capability (A1 5754) in the part contacting the impactor allowed the joint to deflect more and the applied impact energy to be covered by the deformation of the adherends and the adhesive layer. There was good agreement between the experimental and numerical values of axial separation and central deflection. Modeling the adherends and middle region of adhesive with the elastic–plastic material model provided the estimation of the deflection values of the joints close to the experimental results. Cohesive zone parameters are effective in estimating the axial separation value close to experimental results.

Damage Initiation and Propagation Mechanism

When the experimental fracture surfaces were examined, residual adhesive was detected on both the top and bottom adherend surfaces (Fig. 11). This observation was an important resource in establishing the numerical adhesive model. After it was seen that the damage occurred in the adherend–adhesive interface or in the adhesive layer, this damage mechanism was transferred to the numerical model. For this purpose, the adhesive region was divided into three parts [Fig. 2(b)]. Cohesive elements consisted of one piece throughout the thickness, and two separate cohesive elements cannot be joined by touching each other. Considering this, the adherend–adhesive interfaces were modeled with the cohesive zone model and the middle part of adhesive with the elastic–plastic material model. Thanks to this adhesive model and the cohesive parameters used, the axial separation value could be determined close to the experimental results.

It is of great importance for joint design to obtain information about adhesive damage initiation and propagation by examining adhesive damage surfaces. Furthermore, this study aimed to determine the effect of materials with different mechanical properties (Al 2024, Al 5754) on adhesive damage types. After the impact test, in order to examine the types of adhesive damage that occurred in the joints, the damaged surfaces were marked, and the joints were completely separated by hand. The fracture surfaces of the dissimilar joints with overlap length of 40 mm under oblique impact angles are shown in Fig. 11. In addition, the failure types of all the joints are summarized in Table 3. Axial separation values were placed next to the top fracture surface with a gray bar. Adhesive damage is generally characterized in the form of interface, cohesive, and mixed damage modes. Adhesive damage was not observed in the T Al 2024–B Al 5754 joints under 3 J impact energy, except for the 10° impact angle. Applied impact energy was mostly met by the plastic deformation of the adherends. However, the top interface and mixed damage types were commonly seen in the T Al 5754–B Al 2024 joints under the same impact energy. The adhesive damage type occurred as the top interface with the increase in impact energy and impact angle. The increase in impact energy not only increased the speed of initiation and propagation of the adhesive

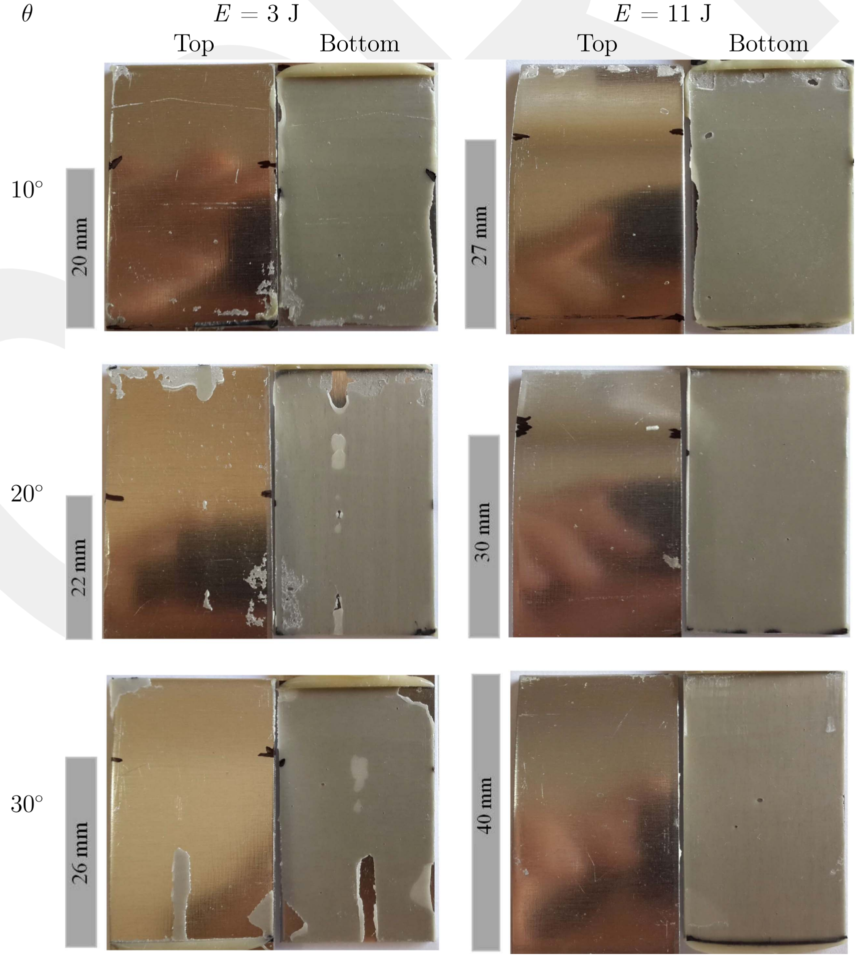

Fig. 11. Fracture surfaces of the top and bottom adherends of T Al 5754–B Al 2024 single-lap joints for different impact angles ($b = 40$ mm).

damage but also affected the adhesive damage mechanism. Because the tangential contact force became more effective with the increase in impact angle, adhesive damage occurred between the top adherend and adhesive interface. In all joints where adhesive damage occurred, the adhesive damage initiated from the right free edge and propagated along the direction of the overlap (Fig. 8). Besides the impact energy and the impact angle, the position (top and bottom) of dissimilar materials (Al 2024, Al 5754) in the joint also affected the adhesive damage type. The effect of the joint configuration, impact angle, and impact energy on the adhesive damage initiation and propagation is shown with time-dependent damage surfaces in Figs. 12 and 13.

In addition, time-dependent axial separation (Δ) graphs of the dissimilar joints are presented in Fig. 14. Adhesive damage propagation was determined using the damage index (SDEG). The damage index has values ranging from 0 to 1, with 0 representing an undamaged element and 1 representing a completely damaged element. Initiation and propagation of the adhesive damage in

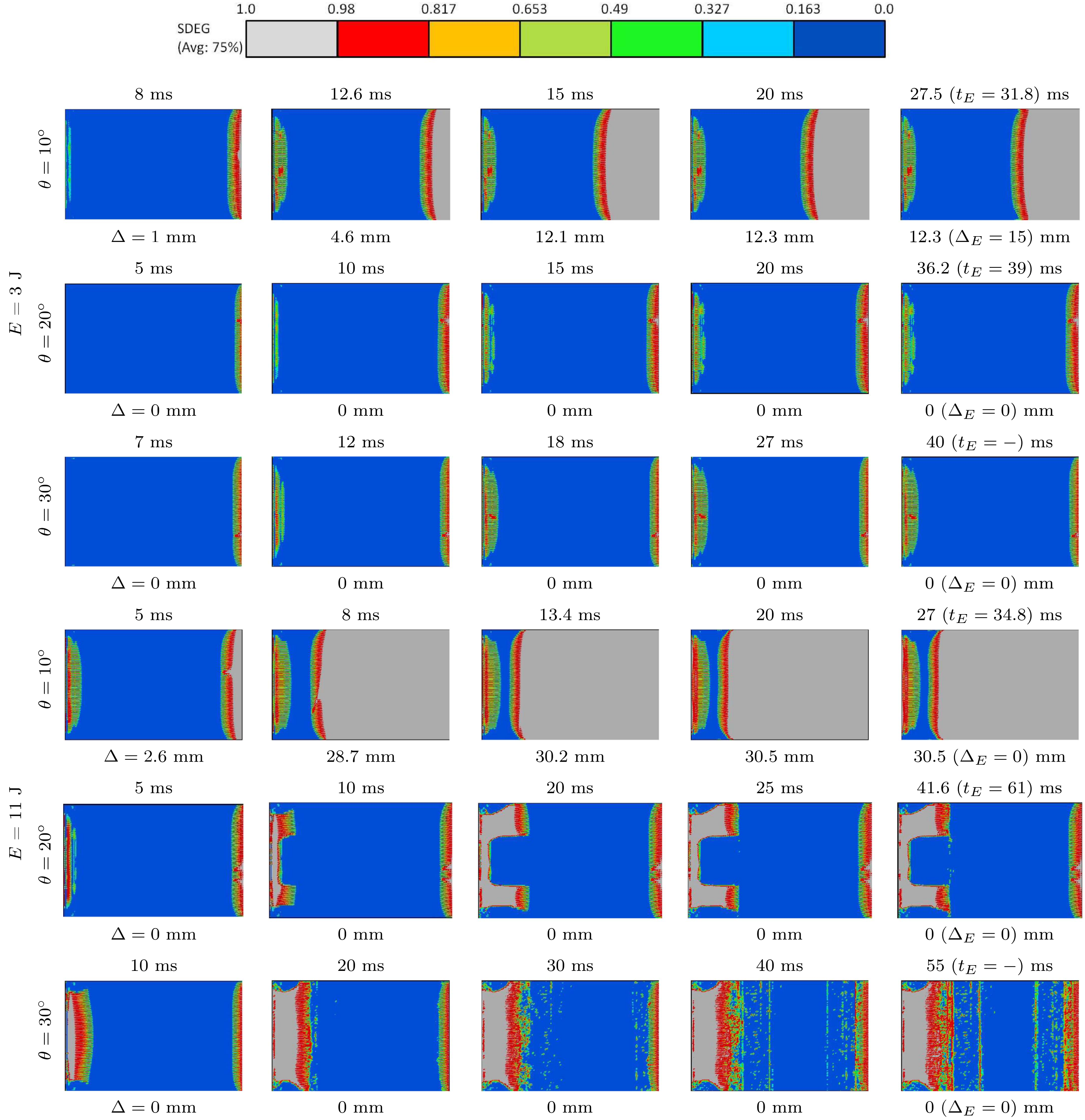

Fig. 12. Numerical damage initiation and propagation along the top adhesive interface of T Al 2024–B Al 5754 single-lap joints ($b = 40$ mm, $E = 3$, 11 J).

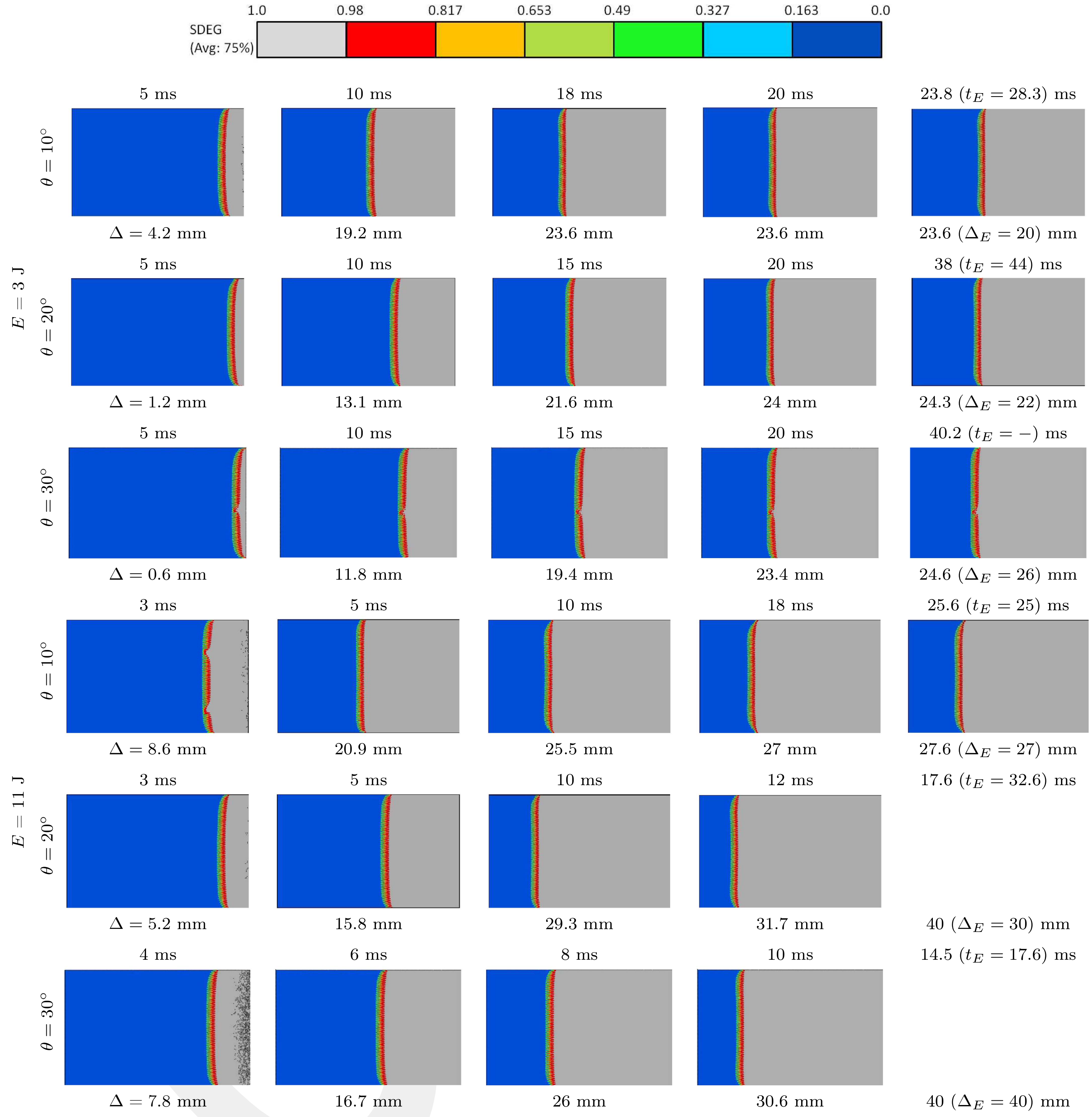

Fig. 13. Numerical damage initiation and propagation along the top adhesive interface of T Al 5754–B Al 2024 single-lap joints ($b = 40$ mm, $E = 3,\ 11$ J).

all joints occurred in the top cohesive region. At 3 J impact energy, the adhesive damage initiated within the first 5 ms, and an increase in impact energy and impact angle caused earlier initiation of adhesive damage. Because of Poisson's effect, the adhesive damage progressed from the outer edges to the middle region and initiated from the right free edge of the overlap region. The use of the cohesive zone model in the interfaces and the elastic–plastic material model in the middle region provided reasonably successful results of adhesive damage initiation and propagation. The adhesive damage zone increased with the increase in the impact angle. The effect of the dissimilar joint configuration, impact angle, impact energy, and overlap length on the adhesive damage propagation is shown in Fig. 14. No adhesive damage occurred in many of the T Al 2024–B Al 5754 joints. Because Al 2024 has a low plastic deformation capacity, the peel stress was reduced in the overlap region, and consequently adhesive damage was reduced. Adhesive damage occurred in the left free zone of the overlap region at high impact energy (11 J) and high impact angle (20°, 30°) for the T Al

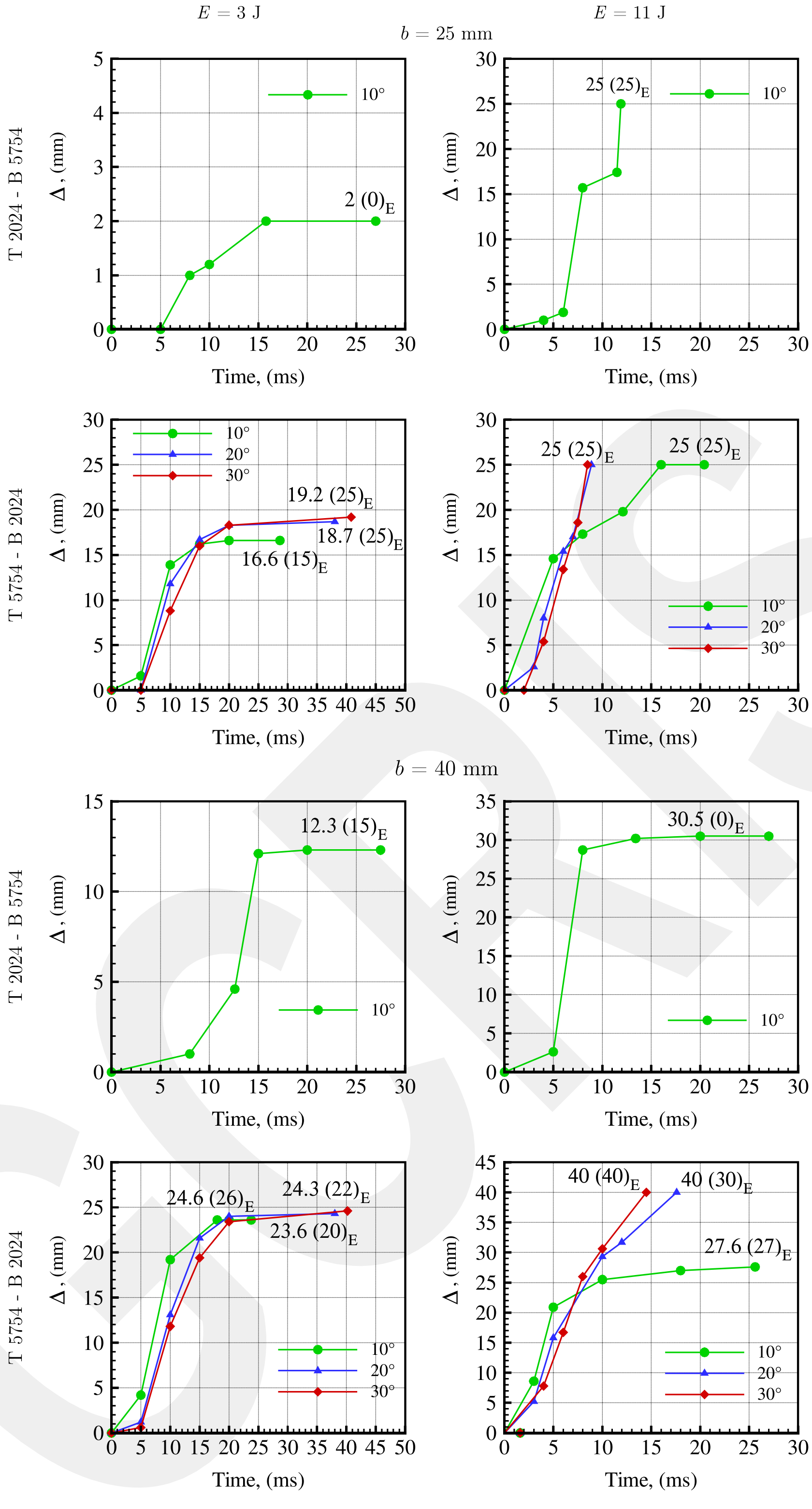

Fig. 14. Axial numerical separation (Δ) variations versus time for dissimilar single-lap joints having different oblique impact angles.

2024–B Al 5754 joints. The increase in impact angle and energy increased the intensity of shear stress at the free edges of the overlap region. In addition, with the deformation of the Al 5754 material (bottom), which has a high plastic deformation capability, peeling stress concentrations occurred on the left free edge of the overlap region, and as a result, adhesive damage occurred in this region. For the T Al 5754–B Al 2024 joints, Al 5754 material with low strength and high plastic deformation capacity decreased the damage propagation rate. However, Al 5754 increased the axial separation length with the effect of peeling due to the plastic deformation it underwent. The mechanical properties of the adherend materials in the joint and their location in the joint (top and bottom) significantly affected the amount of adhesive damage and propagation rate.

J. Aerosp. Eng., 2022, 35(5): 04022075

The increase in the impact energy and angle was another main factor that increased the damage propagation rate. As a result of the increased shear stresses in the overlap region with the increase in impact angle, the adhesive damage initiated in a shorter time. For 11 J impact energy, adhesive damage initiated in the range of 0–5 ms, excluding the 30° impact angle. The increase in impact energy increased both the amount and propagation rate of the adhesive damage. The maximum amount of axial separation occurred in the 0–10 ms time interval with the increase in impact energy. The increase in overlap length not only increased the bending strength of the joint but also increased the adhesive volume where impact energy is met. Therefore, the increase in the overlap length ($b = 40$ mm) increased the amount of axial separation occurring in the joint and decreased the damage propagation rate, especially at high impact energy ($E = 11$ J).

Conclusion

In this study, the behavior of adhesively bonded dissimilar single-lap joints under oblique impact loads was investigated experimentally and numerically by considering the impact angle ($\theta = 10°$, 20°, 30°), overlap length ($b = 25$ and 40 mm), impact energy ($E = 3$ and 11 J), and strength and plastic deformation capability of adherends (Al 2024-T3 and Al 5754-0). The important results obtained in this study are listed in the following.

- There was good agreement between experimental and numerical maximum contact force and deflection values. The contact force decreased with the increase of impact angle in the T Al 2024–B Al 5754 joints, except for the 30° impact angle. In the T Al 5754-B Al 2024 joints, the increase in the impact angle caused a decrease in the contact force value. In addition, the increase in impact energy increased the maximum contact force, deflection, and amount of adhesive damage.
- The lowest adhesive damage occurred in the T Al 2024–B Al 5754 joints. The presence of material with low plastic deformation capacity (Al 2024) in the region in contact with the impactor reduced the peeling effect. In addition, the presence of a material with high plastic deformation capability (Al 5754) in the bottom region enabled the impact energy to be met by the deformation of the bottom adherend material. As a result, adhesive damage was reduced, and the least adhesive damage occurred in the T Al 2024–B Al 5754 joints.
- Adhesive damage initiated from the right free edge of the joint and propagated along the overlap length. The presence of Al 2024 in the region in contact with the impactor generally caused a mixed adhesive damage type, whereas the presence of Al 5754 in the region in contact with the impactor caused adhesive damage to occur along the top adhesive interface due to the peeling effect. In addition, the fact that the material with low plastic deformation ability (Al 2024) was located in the region in contact with the impactor increased the adhesive damage propagation rate.
- The use of the cohesive zone model in the interfaces in contact with the adherends and the elastic–plastic material model in the middle region of adhesive provided reasonable results in predicting the initiation and propagation of adhesive damage and reflected the plasticity effect of the adhesive in the analysis.

Data Availability Statement

Some or all data that support the findings of this study are available from the corresponding author with a reasonable request.

Acknowledgments

The authors thankfully acknowledge the financial support of the Scientific Research Project Division of Erciyes University (BAP) under Contract: FYL-2014-5262.

References

ABAQUS. 2018. "Analysis user's manual, Volume IV: Elements Dassault Systemes (2002–2018)." Accessed June 24, 2022. https://www.3ds.com/.

Abrate, S. 1998. *Impact on composite structures*. Cambridge, UK: Cambridge University Press.

Adams, R. D. 2021. *Adhesive bonding: Science, technology and applications*. Sawston, UK: Woodhead Publishing.

Adams, R. D., J. Comyn, and W. C. Wake. 1997. *Structural adhesive joints in engineering*. New York: Springer.

Alkhatib, S. E., F. Tarlochan, A. Hashem, and S. Sassi. 2018. "Collapse behavior of thin-walled corrugated tapered tubes under oblique impact." *Thin-Walled Struct.* 122 (Nov): 510–528. https://doi.org/10.1016/j.tws.2017.10.044.

Araldite. 2015. "Huntsman advanced materials." Accessed June 24, 2022. https://www.huntsman.com/products/araldite2000/araldite-2015-1.

Araújo, H., J. Machado, E. Marques, and L. Da Silva. 2017. "Dynamic behaviour of composite adhesive joints for the automotive industry." *Compos. Struct.* 171 (Jul): 549–561. https://doi.org/10.1016/j.compstruct.2017.03.071.

Atahan, G. M., and M. K. Apalak. 2017. "Low-speed bending impact behavior of adhesively bonded single-lap joints." *J. Adhes. Sci. Technol.* 31 (14): 1545–1575. https://doi.org/10.1080/01694243.2016.1264105.

Avendaño, R., R. J. C. Carbas, F. J. P. Chaves, M. Costa, L. F. M. Da Silva, and A. A. Fernandes. 2016. "Impact loading of single lap joints of dissimilar lightweight adherends bonded with a crash-resistant epoxy adhesive." *J. Eng. Mater. Technol.* 138 (4): 041019. https://doi.org/10.1115/1.4034204.

Bayramoglu, S., S. Akpinar, and A. Çalık. 2021. "Numerical analysis of elasto-plastic adhesively single step lap joints with cohesive zone models and its experimental verification." *J. Mech. Sci. Technol.* 35 (2): 641–649. https://doi.org/10.1007/s12206-021-0124-0.

Boling, H., and G. Dongyun. 2018. "Dynamic analysis of single-lap, adhesively bonded composite-titanium joints subjected to solid projectile impact." *J. Adhes. Sci. Technol.* 32 (11): 1176–1199. https://doi.org/10.1080/01694243.2017.1404667.

Camanho, P. P., and C. G. Dávila. 2002. *Mixed-mode decohesion finite elements for the simulation of delamination in composite materials*. Technical Rep. No. NASA/TM-2002-211737. Hampton, VA: National Aeronautics and Space Administration.

Campilho, R., M. Banea, J. Neto, and L. da Silva. 2013. "Modelling adhesive joints with cohesive zone models: Effect of the cohesive law shape of the adhesive layer." *Int. J. Adhes. Adhes.* 44 (Jul): 48–56. https://doi.org/10.1016/j.ijadhadh.2013.02.006.

Campilho, R., M. De Moura, D. A. Ramantani, J. Morais, and J. Domingues. 2010. "Buckling strength of adhesively-bonded single and double-strap repairs on carbon-epoxy structures." *Compos. Sci. Technol.* 70 (2): 371–379. https://doi.org/10.1016/j.compscitech.2009.11.010.

Campilho, R. D., M. De Moura, and J. Domingues. 2008. "Using a cohesive damage model to predict the tensile behaviour of CFRP single-strap repairs." *Int. J. Solids Struct.* 45 (5): 1497–1512. https://doi.org/10.1016/j.ijsolstr.2007.10.003.

Chen, Y., M. Li, X. Yang, and W. Luo. 2020. "Damage and failure characteristics of CFRP/aluminum single lap joints designed for lightweight applications." *Thin-Walled Struct.* 153 (Aug): 106802. https://doi.org/10.1016/j.tws.2020.106802.

Dhaliwal, G., and G. Newaz. 2021. "Low-velocity impact characteristics of hybrid aluminum/CFRP single hat sectioned beam adhesively bonded using adhesive tape." *J. Dyn. Behav. Mater.* 7 (3): 383–402. https://doi.org/10.1007/s40870-020-00277-1.

Goldoni, G., and S. Mantovani. 2021. "Damage modelling strategies for unidirectional laminates subjected to impact using CZM and orthotropic plasticity law." *Compos. Struct.* 275 (Nov): 114493. https://doi.org/10.1016/j.compstruct.2021.114493.

Hazimeh, R., G. Challita, K. Khalil, and R. Othman. 2015. "Influence of dissimilar adherends on the stress distribution in adhesively bonded composite joints subjected to impact loadings." *Mech. Compos. Mater.* 50 (6): 717–724. https://doi.org/10.1007/s11029-015-9460-4.

Ivanez, I., M. M. Moure, S. K. Garcia-Castillo, and S. Sanchez-Saez. 2015. "The oblique impact response of composite sandwich plates." *Compos. Struct.* 133 (Dec): 1127–1136. https://doi.org/10.1016/j.compstruct.2015.08.035.

Jairaja, R., and G. N. Naik. 2019. "Single and dual adhesive bond strength analysis of single lap joint between dissimilar adherends." *Int. J. Adhes. Adhes.* 92 (Jul): 142–153. https://doi.org/10.1016/j.ijadhadh.2019.04.016.

Kadioglu, F., and R. D. Adams. 2015. "Flexible adhesives for automotive application under impact loading." *Int. J. Adhes. Adhes.* 56 (Jan): 73–78. https://doi.org/10.1016/j.ijadhadh.2014.08.001.

Kanani, A. Y., X. Hou, R. Laidlaw, and J. Ye. 2021. "The effect of joint configuration on the strength and stress distributions of dissimilar adhesively bonded joints." *Eng. Struct.* 226 (Jan): 111322. https://doi.org/10.1016/j.engstruct.2020.111322.

Kinloch, A. J. 2012. *Adhesion and adhesives: Science and technology*. New York: Springer.

Li, Y., Y. Yang, J. Li, B. Wang, and Y. Liao. 2020. "Experimental-numerical analysis of failure of adhesively bonded lap joints under transverse impact and different temperatures." *Int. J. Impact Eng.* 140 (Jun): 103541. https://doi.org/10.1016/j.ijimpeng.2020.103541.

Liao, L., T. Sawa, and C. Huang. 2013. "Experimental and FEM studies on mechanical properties of single-lap adhesive joint with dissimilar adherends subjected to impact tensile loadings." *Int. J. Adhes. Adhes.* 44 (Jul): 91–98. https://doi.org/10.1016/j.ijadhadh.2013.02.007.

Lißner, M., B. Erice, E. Alabort, D. Thomson, H. Cui, C. Kaboglu, B. R. K. Blackman, M. Gude, and N. Petrinic. 2020. "Multi-material adhesively bonded structures: Characterisation and modelling of their rate-dependent performance." *Composites, Part B* 195 (Aug): 108077. https://doi.org/10.1016/j.compositesb.2020.108077.

Machado, J., E. Marques, M. Silva, and L. F. da Silva. 2018a. "Numerical study of impact behaviour of mixed adhesive single lap joints for the automotive industry." *Int. J. Adhes. Adhes.* 84 (Aug): 92–100. https://doi.org/10.1016/j.ijadhadh.2018.02.036.

Machado, J., P. Nunes, E. Marques, and L. F. da Silva. 2019. "Adhesive joints using aluminium and CFRP substrates tested at low and high temperatures under quasi-static and impact conditions for the automotive industry." *Composites, Part B* 158 (Feb): 102–116. https://doi.org/10.1016/j.compositesb.2018.09.067.

Machado, J., P. Nunes, E. Marques, and L. F. da Silva. 2020. "Numerical study of similar and dissimilar single lap joints under quasi-static and impact conditions." *Int. J. Adhes. Adhes.* 96 (Jan): 102501. https://doi.org/10.1016/j.ijadhadh.2019.102501.

Machado, J. J. M., E. A. S. Marques, and L. F. M. da Silva. 2018b. "Adhesives and adhesive joints under impact loadings: An overview." *J. Adhes.* 94 (6): 421–452. https://doi.org/10.1080/00218464.2017.1282349.

Mittal, K. L. 2012. *Adhesive joints: Formation, characteristics, and testing*. New York: Springer.

Nejad, R. M., D. G. Moghadam, M. Hadi, P. Zamani, and F. Berto. 2022. "An investigation on static and fatigue life evaluation of grooved adhesively bonded t-joints." In Vol. 35 of *Structures*, 340–349. Amsterdam, Netherlands: Elsevier.

Ozdemir, O., and N. Oztoprak. 2017. "An investigation into the effects of fabric reinforcements in the bonding surface on failure response and transverse impact behavior of adhesively bonded dissimilar joints." *Composites, Part B* 126 (Oct): 72–80. https://doi.org/10.1016/j.compositesb.2017.06.005.

Pascal, F., A. Rogani, B. Mahmoud, P. Navarro, S. Marguet, and J.-F. Ferrero. 2018. "Impact damage prediction in thin woven composite laminates—Part II: Application to normal and oblique impacts on sandwich structure." *Compos. Struct.* 190 (Apr): 43–51. https://doi.org/10.1016/j.compstruct.2018.02.013.

Ri, J.-H., M.-H. Kim, and H.-S. Hong. 2022. "A mixed mode elasto-plastic damage model for prediction of failure in single lap joint." *Int. J. Adhes. Adhes.* 116 (Jul): 103134. https://doi.org/10.1016/j.ijadhadh.2022.103134.

Song, J. 2013. "Numerical simulation on windowed tubes subjected to oblique impact loading and a new method for the design of obliquely loaded tubes." *Int. J. Impact Eng.* 54 (Apr): 192–205. https://doi.org/10.1016/j.ijimpeng.2012.11.005.

Sun, G., X. Liu, G. Zheng, Z. Gong, and Q. Li. 2018. "On fracture characteristics of adhesive joints with dissimilar materials—An experimental study using digital image correlation (DIC) technique." *Compos. Struct.* 201 (Oct): 1056–1075. https://doi.org/10.1016/j.compstruct.2018.06.018.

Valente, J., R. Campilho, E. Marques, J. Machado, and L. da Silva. 2019. "Adhesive joint analysis under tensile impact loads by cohesive zone modeling." *Compos. Struct.* 222 (Aug): 110894. https://doi.org/10.1016/j.compstruct.2019.110894.

Wong, K. J. 2013. "Moisture absorption characteristics and effects on mechanical behaviour of carbon/epoxy composite: Application to bonded patch repairs of composite structures." Ph.D. thesis, Dept. of Mechanics, Université de Bourgogne.

Yildirim, M., and M. K. Apalak. 2011. "Transverse low-speed impact behavior of adhesively bonded similar and dissimilar clamped plates." *J. Adhes. Sci. Technol.* 25 (1–3): 69–91. https://doi.org/10.1163/016942410X501106.

You, M., M.-B. Li, Y.-L. Yuan, G. Lin, F.-W. Ma, L.-F. Du, and S.-J. Tang. 2020. "Review of experimental techniques for impact property of adhesive bonds." *Int. J. Adhes. Adhes.* 100 (Jul): 102620. https://doi.org/10.1016/j.ijadhadh.2020.102620.

Zhao, L., Y. Gong, J. Zhang, Y. Chen, and B. Fei. 2014. "Simulation of delamination growth in multidirectional laminates under mode I and mixed mode I/II loadings using cohesive elements." *Compos. Struct.* 116 (Sep): 509–522. https://doi.org/10.1016/j.compstruct.2014.05.042.